POAC'25
St. John's, Newfoundland and Labrador, Canada

Proceedings of the 28th International Conference on Port and Ocean Engineering under Arctic Conditions
Jul 13-17, 2025
St. John's, Newfoundland and Labrador Canada

A Hydrodynamics-Enabled Collision Model for Floating Objects

Marius Seidl[1], Bruce W. T. Quinton[1], Kevin Murrant[2] and Andrew Vardy[1]
[1] Memorial University of Newfoundland, St. John's, Canada
[2] National Research Council – Ocean, Coastal and River Engineering, St. John's, Canada

ABSTRACT

When ships navigate through ice-covered waters they may interact with the ice floes, either by direct ship-ice collisions or by disturbing the floes, indirectly causing ice-ice collisions. Numerical simulations used in ship navigation in ice and to develop autopilots for these situations require physical models of such collisions that account for the multitude of hydrostatic and hydrodynamic phenomena present. So far, the kinematics of collisions between floating objects has only been considered under the assumption that the coupling between axes for hydrodynamic effects can be neglected. Here we introduce a hydrodynamics-enabled collision model for floating objects that allows the consideration of a 6×6 added mass tensor with up to 36 distinct entries. Collisions are treated as instantaneous events in an impulse-based framework. A parameter study reveals significant differences between our model and a model with neglected hydrodynamic coupling, even at low to moderate values of the added mass coupling terms. The prediction of the velocity changes in real-world collision events between a floating dock and a model scale platform supply vessel show that our model captures the correct trends for the linear modes of motion.

KEY WORDS: Collision; Added Mass; Hydrodynamics; Algorithm; Floating Objects.

INTRODUCTION

Kinematic simulations try to model and thus predict the motion of objects in space over time. In multibody kinematic simulations the influence of interactions between multiple objects on their individual motion is of central interest. Direct collisions are a very common type of interaction and thus collision models are a crucial component of such multibody kinematic simulations. Generally, collision models can be either instantaneous (impulse-based) or continuous (force-based) and either include or neglect frictional effects (Seifried *et al.* 2010; Pfeiffer and Glocker 1996).

For ships and other floating objects hydrostatic and hydrodynamic effects need to be modelled for a high-fidelity simulation (Fossen, 2002). The governing equations for collision responses are dominated by mass and moment of inertia, thus added mass is the crucial hydrodynamic effect that needs to be included in a collision model for ships and floating objects (Liu and Soares, 2023).

Previous work has mostly focused on deformation and damage due to collisions between floating structures. Thus, continuous collision models were used, and kinematic accuracy was not the major concern of these studies (Liu and Soares, 2023). For the navigation of ships in ice with only safe interactions, the rigid body assumption (i.e. neglectable deformations) may hold and high-fidelity kinematic models are desirable, since they can be used for path planning, development of autopilots, etc. (Fossen, 2002). Baraff and Witkin (1997) provided a detailed general introduction to the

computational approach of resolving collisions in a 6 degree of freedom DOF impulse-based framework, without considering hydrodynamic effects.

Peterson (1982) described a 3 DOF, frictionless, continuous collision model focused on the assessment of deformations that considers a system with decoupling between the surge, and sway-yaw subsystems and includes the added mass for both subsystems. Liu and Amdahl (2010) introduced frictional effects to an otherwise similar model and applied it to ship-iceberg collisions. Song *et al.* (2016) focused on ice-structure interactions as well, with an emphasis on sway added mass. Their model is the first to introduce a proximity dependence of the added mass during the collision, as theoretically expected (Korotkin, 2009). Yu *et al.* (2016) described a collision model extended to 6 DOF that uses a diagonal added mass tensor. Yu *et al.* (2016b) used state of the art computational fluid dynamics methods to access the damage of ship-ship collisions and ship grounding events in 6 DOF, still considering solely a diagonal added mass tensor in their simulations. Recently, Liu and Amdahl (2019) unified the theoretical contributions of previous work on 6 DOF ship-ship collisions. Their work includes different frictional effects and hydrodynamic effects. The latter are modelled with constant added mass factors that do not include any coupling between the different axes. To the best of our knowledge, a full 6×6 added mass tensor has not yet been used in any collision resolution method.

THEORY DERIVATION

For the derivation of our new, original collision response model using the full added mass tensor an inelastic, instantaneous and frictionless interaction between the colliding objects is assumed.

Some care must be taken with respect to the frames of reference used during the following derivation. Linear velocities $\mathbf{v}$ and angular velocities $\boldsymbol{\omega}$ of a given object are expressed by the motion of the frame of reference of the object (fixed at the respective origins) with respect to a world frame (which is assumed to be inertial). Independent of the particular choice of origin $\mathcal{O}$, the velocity $\mathbf{v_p}$ of a point $\mathbf{p}$ of an object with respect to the origin is given by

$$\mathbf{v_p} = \mathbf{v}_{\mathcal{O}} + \boldsymbol{\omega} \times {}^{\mathcal{O}}\mathbf{p} \tag{1}$$

with the left superscript indicating the frame of reference of a variable. The system inertia tensor

$$\mathbf{M} = \mathbf{M}_{\mathrm{RB}} + \mathbf{M}_{\mathrm{A}} \tag{2}$$

can be separated into a rigid body part $\mathbf{M}_{\mathrm{RB}}$ and the hydrodynamic added mass part $\mathbf{M}_{\mathrm{A}}$**.** When looking at a rigid body in water, the choice of the origin of the coordinate frame is particularly important. The following derivation of the proposed collision resolution strategy relies on choosing the center of gravity CG as origin. With this choice, the rigid body system inertia matrix takes the favourable shape

$${}^{\mathrm{CG}}\mathbf{M}_{\mathrm{RB}} = \begin{bmatrix} m\mathbf{I}_{3\times3} & \mathbf{0}_{3\times3} \\ \mathbf{0}_{3\times3} & {}^{\mathrm{CG}}\boldsymbol{\Gamma} \end{bmatrix} \tag{3}$$

with the inertia tensor ${}^{\mathrm{CG}}\boldsymbol{\Gamma}$ with respect to CG. Since the added mass depends on the geometry of the floating object, no such favourable shape can be exploited for the added mass part of the system inertia tensor. The appropriate transformations to change the origin of a system inertia tensor or its components to CG to then use the here proposed collision resolution strategy is given in Fossen (2002).

The equations of motion for floating objects in vector notation with CG as origin (from hereon forward the superscript for CG as the chosen origin for $\mathbf{M}$ is implied for clarity of equations) can be written as

$$\mathbf{M}\begin{bmatrix} \mathrm{d}\mathbf{v}/\mathrm{d}t \\ \mathrm{d}\boldsymbol{\omega}/\mathrm{d}t \end{bmatrix} + \mathbf{C}(\mathbf{v},\boldsymbol{\omega})\begin{bmatrix} \mathbf{v} \\ \boldsymbol{\omega} \end{bmatrix} + \mathbf{D}(\mathbf{v},\boldsymbol{\omega})\begin{bmatrix} \mathbf{v} \\ \boldsymbol{\omega} \end{bmatrix} = \begin{bmatrix} \mathbf{f} \\ \boldsymbol{\tau} \end{bmatrix} \tag{4}$$

with $\mathbf{C}$ the Coriolis-centripetal tensor, $\mathbf{D}$ the damping tensor and a vector containing the forces $\mathbf{f}$ and moments $\boldsymbol{\tau}$. Forces and moments consist of control inputs, ballast pre-trimming, environmental disturbances and the negative of the gravitational and buoyancy forces and moments, which sum up to $[\mathbf{f} \quad \boldsymbol{\tau}]^{\top}$ (Fossen, 2002).

This equation simplifies significantly under the assumption of an instantaneous collision. All aforementioned forces and moments tend to $\mathbf{0}$ for an infinitesimal time interval. The same is true for $[\mathbf{v} \quad \boldsymbol{\omega}]^\mathsf{T}$ which can be written as differential $[\mathrm{d}\mathbf{x}/\mathrm{d}t \quad \mathrm{d}\boldsymbol{\chi}/\mathrm{d}t]^\mathsf{T}$ with changes in position $\mathbf{x}$ and orientation $\boldsymbol{\chi}$ both tending towards $\mathbf{0}$ during an infinitesimal time interval. Finally, with the assumption of a single, infinitesimal points of contact, we can set $\boldsymbol{\tau} = \mathbf{0}$ and use the simplified equation

$$\mathbf{M}\begin{bmatrix}\mathrm{d}\mathbf{v}/\mathrm{d}t\\ \mathrm{d}\boldsymbol{\omega}/\mathrm{d}t\end{bmatrix} = \begin{bmatrix}\mathbf{f}\\ \mathbf{0}\end{bmatrix} \tag{5}$$

which describes the motion of each single collision partner at the instant of collision. Integration with respect to time yields the relationship between collision impulse $\mathbf{j}$ and velocity changes $\Delta\mathbf{v}$ and $\Delta\boldsymbol{\omega}$ as

$$\begin{bmatrix}\Delta\mathbf{v}\\ \Delta\boldsymbol{\omega}\end{bmatrix} = \mathbf{M}^{-1}\begin{bmatrix}\mathbf{j}\\ \mathbf{0}\end{bmatrix} = \begin{bmatrix}\mathbf{M}_{11} & \mathbf{M}_{12}\\ \mathbf{M}_{22} & \mathbf{M}_{22}\end{bmatrix}^{-1}\begin{bmatrix}\mathbf{j}\\ \mathbf{0}\end{bmatrix} = \begin{bmatrix}(\mathbf{M}_{11}-\mathbf{M}_{12}\mathbf{M}_{22}^{-1}\mathbf{M}_{21})^{-1}\\ -\mathbf{M}_{22}^{-1}\mathbf{M}_{21}(\mathbf{M}_{11}-\mathbf{M}_{12}\mathbf{M}_{22}^{-1}\mathbf{M}_{21})^{-1}\end{bmatrix}\mathbf{j} \tag{6}$$

with the last decomposition using block matrix identities and the fact that the impulse vector is part $\mathbf{0}$.

Since the system inertia tensor with CG as origin ${}^{\mathrm{CG}}\mathbf{M}$ is used, we know that ${}^{\mathrm{CG}}\mathbf{M}_{\mathrm{RB},21} = \mathbf{0}_{3\times3}$. Thus, only $\mathbf{M}_\mathrm{A}$ contributes to $\Delta\boldsymbol{\omega}$ in equation 6 and we can separate the change in angular velocity

$$\Delta\boldsymbol{\omega} = \Delta\boldsymbol{\omega}_\mathrm{geo} + \Delta\boldsymbol{\omega}_\mathrm{A} \tag{7}$$

into a geometric part $\Delta\boldsymbol{\omega}_\mathrm{geo}$ and an added mass part $\Delta\boldsymbol{\omega}_\mathrm{A}$, with the latter given by equation 6.

Following Baraff and Witkin (1997) the geometric portion is given by

$$\Delta\boldsymbol{\omega}_\mathrm{geo} = \overrightarrow{\boldsymbol{\omega}}_\mathrm{geo} - \overleftarrow{\boldsymbol{\omega}}_\mathrm{geo} = \mathbf{M}_{22}^{-1}({}^{\mathrm{CG}}\mathbf{p}\times\mathbf{j}) \tag{8}$$

with the right-pointing arrow indicating the post- and the left-pointing arrow indicating the pre-collision quantity. Writing the collision impulse as a scalar multiplied by the contact normal ($\mathbf{j} = j\,{}^{\mathrm{CG}}\mathbf{n}$) the collision impulse can be worked out from

$$\begin{aligned}\vec{\mathbf{v}}_\mathrm{CG} &= \overleftarrow{\mathbf{v}}_\mathrm{CG} + (\mathbf{M}_{11}-\mathbf{M}_{12}\mathbf{M}_{22}^{-1}\mathbf{M}_{21})^{-1}j\,{}^{\mathrm{CG}}\mathbf{n}\\ \overrightarrow{\boldsymbol{\omega}}_\mathrm{CG} &= \overleftarrow{\boldsymbol{\omega}}_\mathrm{CG} - \mathbf{M}_{22}^{-1}\mathbf{M}_{21}(\mathbf{M}_{11}-\mathbf{M}_{12}\mathbf{M}_{22}^{-1}\mathbf{M}_{21})^{-1}j\,{}^{\mathrm{CG}}\mathbf{n} + \mathbf{M}_{22}^{-1}({}^{\mathrm{CG}}\mathbf{p}\times j\,{}^{\mathrm{CG}}\mathbf{n})\end{aligned} \tag{9}$$

which is the combination of equations 6-8 and finally used to calculate the post collision velocities.

Substituting equation 9 into equation 1 for the post-collision velocity yields

$$\begin{aligned}\vec{\mathbf{v}}_\mathbf{p} &= \overleftarrow{\mathbf{v}}_\mathrm{CG} + (\mathbf{M}_{11}-\mathbf{M}_{12}\mathbf{M}_{22}^{-1}\mathbf{M}_{21})^{-1}j\,{}^{\mathrm{CG}}\mathbf{n}\\ &\quad + \left(\overleftarrow{\boldsymbol{\omega}}_\mathrm{CG} - \mathbf{M}_{22}^{-1}\mathbf{M}_{21}(\mathbf{M}_{11}-\mathbf{M}_{12}\mathbf{M}_{22}^{-1}\mathbf{M}_{21})^{-1}j\,{}^{\mathrm{CG}}\mathbf{n} + \mathbf{M}_{22}^{-1}({}^{\mathrm{CG}}\mathbf{p}\times j\,{}^{\mathrm{CG}}\mathbf{n})\right)\times{}^{\mathrm{CG}}\mathbf{p}\\ &= \overleftarrow{\mathbf{v}}_\mathrm{CG} + \overleftarrow{\boldsymbol{\omega}}_\mathrm{CG}\times{}^{\mathrm{CG}}\mathbf{p} + (\mathbf{M}_{11}-\mathbf{M}_{12}\mathbf{M}_{22}^{-1}\mathbf{M}_{21})^{-1}j\,{}^{\mathrm{CG}}\mathbf{n}\\ &\quad + \left(-\mathbf{M}_{22}^{-1}\mathbf{M}_{21}(\mathbf{M}_{11}-\mathbf{M}_{12}\mathbf{M}_{22}^{-1}\mathbf{M}_{21})^{-1}j\,{}^{\mathrm{CG}}\mathbf{n} + \mathbf{M}_{22}^{-1}({}^{\mathrm{CG}}\mathbf{p}\times j\,{}^{\mathrm{CG}}\mathbf{n})\right)\times{}^{\mathrm{CG}}\mathbf{p}\\ &= \overleftarrow{\mathbf{v}}_\mathbf{p} + j((\mathbf{M}_{11}-\mathbf{M}_{12}\mathbf{M}_{22}^{-1}\mathbf{M}_{21})^{-1}\,{}^{\mathrm{CG}}\mathbf{n}\\ &\quad +(\mathbf{M}_{22}^{-1}({}^{\mathrm{CG}}\mathbf{p}\times{}^{\mathrm{CG}}\mathbf{n}) - \mathbf{M}_{22}^{-1}\mathbf{M}_{21}(\mathbf{M}_{11}-\mathbf{M}_{12}\mathbf{M}_{22}^{-1}\mathbf{M}_{21})^{-1}\,{}^{\mathrm{CG}}\mathbf{n})\times{}^{\mathrm{CG}}\mathbf{p})\\ &= \overleftarrow{\mathbf{v}}_\mathbf{p} + j\,{}^{\mathrm{CG}}\mathbf{c}_j\end{aligned} \tag{10}$$

which, despite the number of terms to consider, is just a linear expression connecting the pre- and post-collision velocities of a point with a scalar impulse multiplied by a vector constant ${}^{\mathrm{CG}}\mathbf{c}_j$ as indicated in the last line of equation 10. The sign in the equation must be different for the two collision partners and which one is treated as addition and which one as subtraction depends on the convention chosen. Here, the contact normal is set to be pointing outwards from object a and thereby addition is chosen for object a and subtraction for object b.

The pre- and post-collision velocities are obtainable from the state of the objects before or after the collision according to equation 1 knowing the point of contact and the contact normal as

$$\begin{aligned}\overleftarrow{v}_\mathrm{rel} &= {}^{\mathrm{CG}}\mathbf{n}\cdot\left(\overleftarrow{\mathbf{v}}_{\mathbf{p},a} - \overleftarrow{\mathbf{v}}_{\mathbf{p},b}\right)\\ \vec{v}_\mathrm{rel} &= {}^{\mathrm{CG}}\mathbf{n}\cdot\left(\vec{\mathbf{v}}_{\mathbf{p},a} - \vec{\mathbf{v}}_{\mathbf{p},b}\right)\end{aligned} \tag{11}$$

The post-collision quantities are obviously unknown, but the relative velocities pre- and post-collision are connected by the coefficient of restitution c

$$\vec{v}_{\mathrm{rel}} = -c \cdot \overleftarrow{v}_{\mathrm{rel}} \tag{12}$$

so, we can equate

$$\vec{v}_{\mathrm{rel}} = {}^{\mathrm{CG}}\mathbf{n} \cdot \left(\overleftarrow{\mathbf{v}}_{\mathbf{p},a} + j\,{}^{\mathrm{CG}}\mathbf{c}_{j,a} - \overleftarrow{\mathbf{v}}_{\mathbf{p},b} + j\,{}^{\mathrm{CG}}\mathbf{c}_{j,b}\right) = \overleftarrow{v}_{\mathrm{rel}} + j\,{}^{\mathrm{CG}}\mathbf{n} \cdot \left({}^{\mathrm{CG}}\mathbf{c}_{j,a} + {}^{\mathrm{CG}}\mathbf{c}_{j,b}\right) = -c \cdot \overleftarrow{v}_{\mathrm{rel}} \tag{13}$$

which can be solved for the impulse as

$$j = -(1+c)\,\overleftarrow{v}_{\mathrm{rel}} \,/\, {}^{\mathrm{CG}}\mathbf{n} \cdot \left({}^{\mathrm{CG}}\mathbf{c}_{j,a} + {}^{\mathrm{CG}}\mathbf{c}_{j,b}\right)$$

$$\text{With } {}^{\mathrm{CG}}\mathbf{c}_{j,a|b} = \left(\mathbf{M}_{11,a|b} - \mathbf{M}_{12,a|b}\mathbf{M}_{22,a|b}^{-1}\mathbf{M}_{21,a|b}\right)^{-1} {}^{\mathrm{CG}}\mathbf{n} + \left(\mathbf{M}_{22,a|b}^{-1}\left({}^{\mathrm{CG}}\mathbf{p}_{a|b} \times {}^{\mathrm{CG}}\mathbf{n}\right)\right. \tag{14}$$
$$\left. -\mathbf{M}_{22,a|b}^{-1}\mathbf{M}_{21,a|b}\left(\mathbf{M}_{11,a|b} - \mathbf{M}_{12,a|b}\mathbf{M}_{22,a|b}^{-1}\mathbf{M}_{21,a|b}\right)^{-1} {}^{\mathrm{CG}}\mathbf{n}\right) \times {}^{\mathrm{CG}}\mathbf{p}_{a|b}$$

With an equation for j, the procedure to resolve a collision is as follows, assuming the coefficient of restitution is known (or set by the user):

1. Transform system inertia matrix to CG, if not already known w.r.t CG.
2. Gather geometric information about collision: contact point w.r.t. CGs of each body (${}^{\mathrm{CG}}\mathbf{p}_a$ and ${}^{\mathrm{CG}}\mathbf{p}_b$) and contact normal ${}^{\mathrm{CG}}\mathbf{n}$.
3. Calculate pre-collision relative velocity $\overleftarrow{v}_{\mathrm{rel}}$ according to equations 1 and 11.
4. Calculate scalar collision impulse j according to equation 14.
5. Calculate linear velocity change $\Delta\mathbf{v}$ and added mass angular velocity change $\Delta\boldsymbol{\omega}_{\mathrm{A}}$ according to equation 6 and add geometric change of angular velocity $\Delta\boldsymbol{\omega}_{\mathrm{geo}}$ (Eq. 7-8) to angular velocity change and update velocities.

METHODS

For the parameter study, the WAMIT v7 computational package (WAMIT, 2025) was used to determine the added mass tensor of a cube with $a = 10$ cm side length and $m = 1$ kg mass (i.e. just fully submerged, z-position of CG at -5 cm w.r.t. waterline) in wave-free conditions. The cube's moment of inertia in each axis was determined as $I = 1/6ma^2 = 1/600$ kg $\cdot$ m^2, yielding a radius of gyration of $r_g = \sqrt{I/m} \approx 0.040825$ m. The quadrilateral mesh of the cube was procedurally generated from squares with 1 cm^2 resolution.

Collisions between two just fully submerged cubes of unit mass were studied, determining the rigid body system inertia tensor as $\mathrm{diag}([1\ \mathrm{kg}, 1\ \mathrm{kg}, 1\ \mathrm{kg}, 1/600\ \mathrm{kg}\cdot\mathrm{m}^2,\ 1/600\ \mathrm{kg}\cdot\mathrm{m}^2, 1/600\ \mathrm{kg}\cdot\mathrm{m}^2])$. The diagonal elements of the added mass tensor were determined using computer simulation with WAMIT as $\mathrm{diag}([0.525\ \mathrm{kg}, 0.525\ \mathrm{kg}, 0.345\ \mathrm{kg}, 0.00170\ \mathrm{kg}\cdot\mathrm{m}^2, 0.00170\ \mathrm{kg}\cdot\mathrm{m}^2, 0.000417\ \mathrm{kg}\cdot\mathrm{m}^2])$. The off-diagonal terms of the added mass tensor were varied in percent of the minimum value of the two diagonal values of the added mass tensor, that were coupled in a particular axis (e.g. for $M_{A,15}$ at 1%, a off diagonal value of $1\% \cdot \min(0.525, 0.00170)$ was chosen). Note that these are not the actual off-diagonal values of a just fully submerged cube, but values artificially added to the added mass tensor. One may imagine massless fins being attached to the cubes causing the particular coupling resulting in the assumed off-diagonal elements of the added mass tensors.

Due to the complexity of the space of possible geometric arrangements, a particularly interesting subset of it was studied here. The faces of the cubes containing the contact point were assumed to coincide with the xz-plane, while the contact point was chosen from the positive x-axis only (Fig. 1). Note that a single point of contact was assumed, despite the two faces being in closest proximity. One may assume an infinitesimal distance between the two faces with an equally infinitesimal bump in the surface at the contact point. From this arrangement follows the fixed contact normal $n = [0, 1, 0]$.

Further, the first body was assumed to be at rest (i.e. the struck object) with its CG at $[0, -1, 0]$, while the position of the second body, and thus its CG, was varied along the positive x-axis with a y-offset of $+1$ (Fig. 1). Unity relative velocity and coefficient of restitution CoR values were set. To satisfy the velocity value, a velocity vector of $[0, -1, 0, 0, 0, 0]$ of the second body (i.e. the striking object) was chosen. Note that only normal and not tangential components of the velocity are relevant for the collision resolution, as such only the linear velocity along the y-axis and the angular velocities around the x- and z-axis determine the relative velocity.

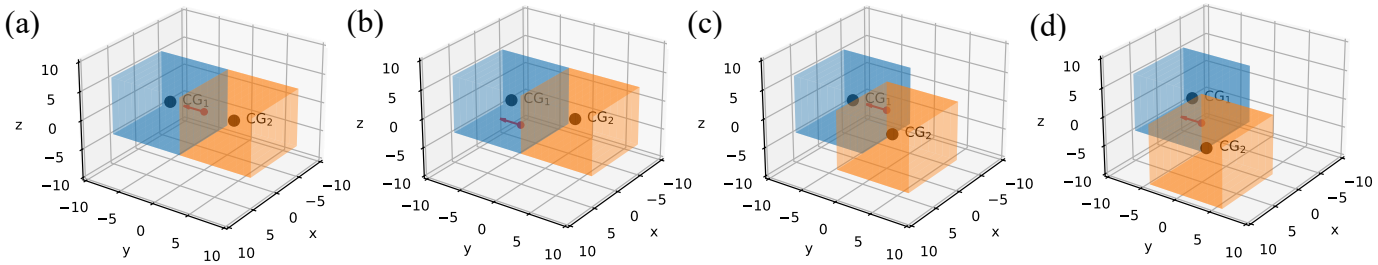

Figure 1: Different geometric situations as varied during the parameter study, with the struck body in blue and the striking body in orange. The velocity vector (red) is anchored at the contact point. (a) CGs and contact point without offset and colinear with velocity vector, (b) offset of contact point, (c) offset of striking body, (d) striking body and contact point offset.

For the experimental study, a generic model scale platform supply vessel PSV (Fig. 2a) was set to collide with a floating dock (Fig. 2b) and their pose in all 6 DOF recorded at a frequency of 50 Hz using a Qualisys motion capture system. The captured pose data was corrected by a known offset to the CG of the PSV and dock, respectively. The physical properties of the PSV and dock are shown in Table 1. The model was positioned relative to the floating dock using a custom control software and accelerated towards the dock until a steady speed at the commanded forward thrust of either 1 N (0.13 ± 0.01 m/s) or 5 N (0.32 ± 0.02 m/s) was reached. The thrust was cut shortly before impact to let the collision evolve naturally. The PSV was positioned such that it would hit the dock with its bow at either the centre C, halfway between centre and edge CE or the edge E (Fig. 2b). For each combination of forward thrust and collision point the experiment was repeated 3 times. Finally, for 3 experimental runs with 5 N forward thrust and the collision point set to CE each a weight of either 10 kg or 20 kg was added to the dock, resulting in a total of 24 experimental runs.

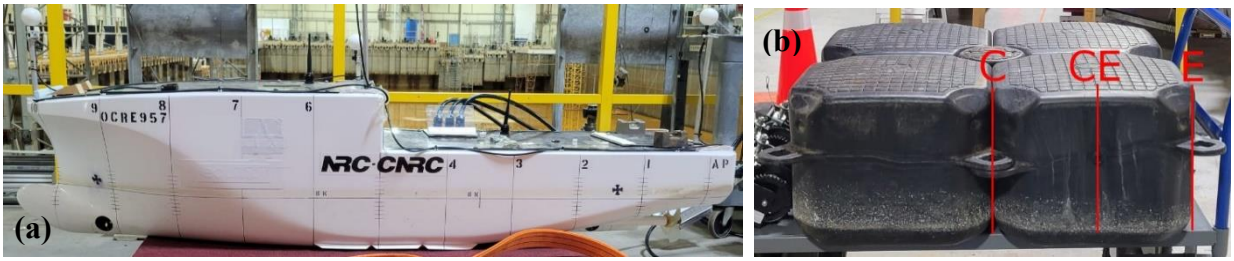

Figure 2: (a) The PSV model, (b) floating dock with position of impact marked.

Table 1: Physical properties of PSV and dock

Property	PSV	Floating dock
Displacement / kg	70.047	44.95
Beam / m	0.45	1.0
Length overall / m	2.0	1.0
Height / m	0.4	0.4
CG to waterline / m	0.042	-0.15

A linear function was fitted to the recorded position and orientation time traces shortly before and after the collision to extract the pre- and post-collision velocities including their uncertainties from the fit's slopes (Fig. 3). The time range for each fit was manually set to a value between $0.1 - 4$ s to select a visibly linear region of the time trace. The intersections of the linear fits for the pre- and post-collision pose were used as an estimate of CG and pose during the time of impact. The uncertainty of CG was calculated by error propagation from the fits' uncertainties.

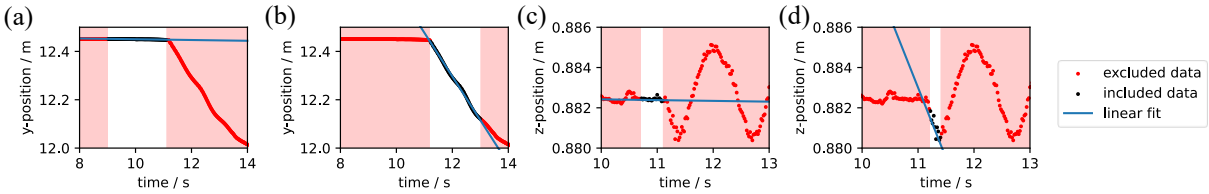

Figure 3: Examples of selected data ranges and linear fits to a single DOF for a linear mode (a, b) and an oscillatory mode (c, d) both pre- (a, c) and post-collision (b, d).

Surface meshes of the floating dock and PSV were positioned in a CAD software according to the previously determined pose at the time of impact and an intersection between the two meshes was calculated. The first point of contact on the intersection was manually estimated and selected and the face normal at the contact point extracted from the mesh. In case of an empty intersection the point closest to the PSV model on the dock's mesh was selected. The error of the manually selected point of contact was assumed to be 0.1 m per axis. The contact normal was assumed to have a standard deviation of its orientation in space of $5°$ per axis.

WAMIT v7 was used with the same settings as described before to determine the added mass tensor of PSV and floating dock. The previously used triangular meshes were smoothed and turned into quadrilateral meshes to be usable by WAMIT. To determine the moment of inertia and consequently the radii of gyration according to $r_g = \sqrt{I/m}$ the floating dock was approximated by a $1\text{ m} \times 1\text{ m} \times 0.4\text{ m}$ box ($w \times d \times h$), which yields $I_x = I_y = 1/12m(d|w^2 + h^2) = 4.345\text{ kg} \cdot \text{m}^2$ and $I_z = 1/12m(d^2 + w^2) = 7.492\text{ kg} \cdot \text{m}^2$. The PSV was modelled as a cylinder with length $l = 2\text{ m}$ and radius $r = 0.25\text{ m}$, yielding moments of inertia of $I_x = 1/2mr^2 = 2.19\text{ kg} \cdot \text{m}^2$ and $I_y = I_z = 1/12m(3r^2 + l^2) = 24.44\text{ kg} \cdot \text{m}^2$. A standard deviation of 1% of each value was assumed for the system inertia tensor of the floating dock and of 2% for the PSV due to the more corse approximation of the PSV's shape for the determination of the moment of inertia.

The CoR was determined based on the kinetic energy E of the system (i.e. both objects) according to $c = \sqrt{E_{post}/E_{pre}} = \sqrt{(E_{post,dock} + E_{post,PSV})/(E_{pre,dock} + E_{pre,PSV})}$ where the kinetic energy of each floating object at each time is given by the sum of the kinetic energy of the rigid body and the fluid as $E_i = v_i^\top M_{RB,i} v_i + v_i^\top M_{A,i} v_i$.

The uncertainty of the theoretical predictions was estimated by a Monte-Carlo approach with 10000 runs each. A random value according to a normal distribution with centre and standard deviation equal to each input value and its estimated error was drawn and used as input to the algorithm. The standard deviation of the output of all runs is the estimate of the error propagation result through the algorithm.

RESULTS

Parameter Study

To analyze the influence of the off-diagonal elements in the added mass tensor on the collision response (i.e. the velocity changes upon a collision) a parameter study was conducted.

From equation 14 it follows that there are four major factors that define the velocity changes upon a collision. The relative pre-collision velocity and the CoR are both scalar factors and as such were set to unity in the parameter study, as they simply scale the velocity change equally along all axes. The other factors are the geometric arrangement of the colliding bodies and the values of the system inertia tensors.

Figure 4 shows the baseline (i.e. all off-diagonal values of the added mass tensor are 0) of the parameter study as a function of the different geometric arrangements over the full range covered. Note that due to the chosen restrictions of the geometric arrangements, only velocity changes in the x-, y- and yaw-axis were analyzed, since the geometry is essentially restricted to 3 DOF.

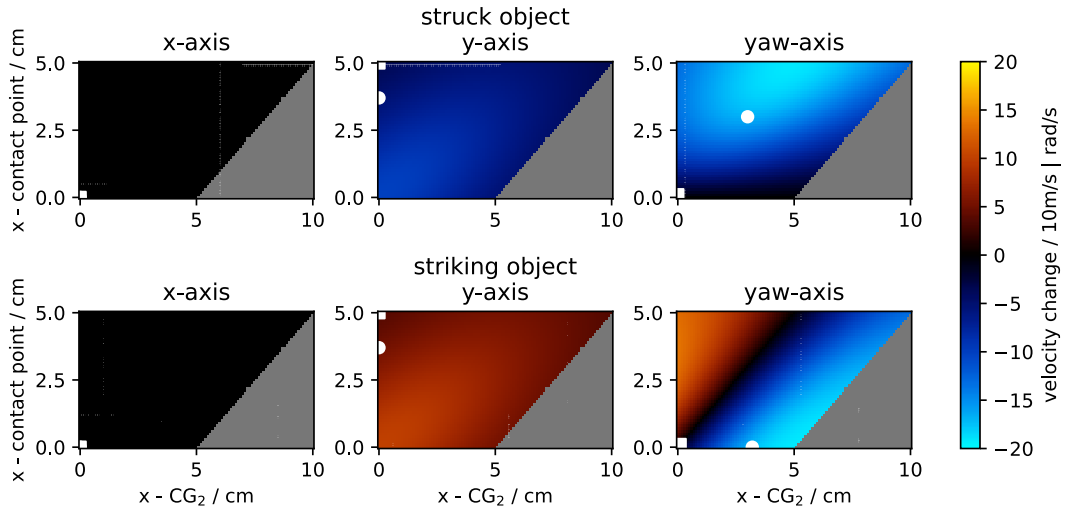

Figure 4: Baseline of the parameter study. (0, 0) corresponds to geometric situation (a), (0, 5) to (b), (5, 0) to (c) and, (10, 5) to (d) in Figure 1. The grey area indicates geometrically impossible arrangements. The arrangement of maximum absolute change per axis is indicated by a white circle, that of the maximum relative change by a white square. For the x-axis both points coincide.

Figure 5 displays the maximum change in velocity relative to the baseline. The geometric situation for each maximum is indicated in Figure 4. If the coupling terms (i.e. off-diagonal elements) of the added mass tensor are 0, the velocity along the x-axis is and stays 0 given the chosen geometric arrangement (Fig. 1 and 4). As such, Figure 5 does not show the change relative to the baseline, but relative to the pre-collision velocity.

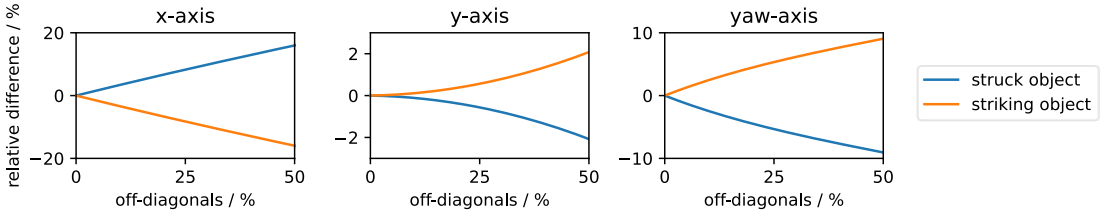

Figure 5: Relative differences between baseline and new theory as a function of the magnitude of the off-diagonal terms in the added mass tensor.

The appearing non-zero velocity in x-direction upon introducing non-zero off-diagonal terms in the added mass tensor is a significant difference between the current standard method as described in the literature and the collision resolution model presented in this paper. This physical effect of a motion solely caused due to hydrodynamic coupling at the time of collision is simply not captured if a diagonal added mass tensor is used.

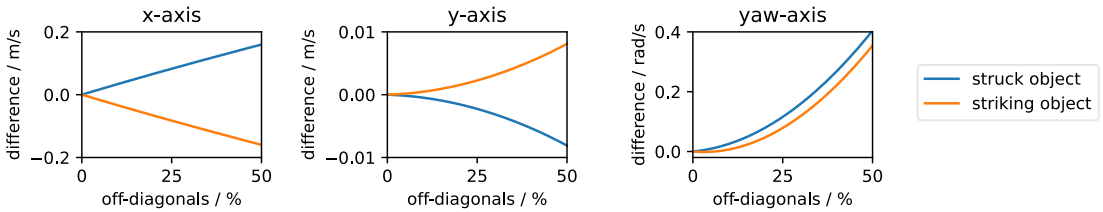

Figure 6: Absolute differences between baseline and new theory as a function of the magnitude of the off-diagonal terms in the added mass tensor.

Figures 5 and 6 further illustrates that the difference between using a diagonal or full added mass tensor with respect to the resulting velocity changes is quite significant. Considering for example the 10% mark of the off-diagonal elements, which are values that certainly can occur in real structures, a maximum change for x of 0.03 m/s or 3%, for y of 0.0004 m/s or 0.1%, and for yaw of 0.007 rad/s or 2% of the velocity response upon a collision is observed.

Figure 7 shows the absolute differences for the 10% mark as a function of geometric arrangement as an example. The trends visible are representative for any percentage of the off-diagonal values. It shows that for the x-axis the strongest effect off the off-diagonal terms is observed for a head-on collision with misalignment in either CG or the contact point resulting in a less strong effect. For the y-axis the effect is reversed, and a strong effect occurs if the misalignment between either or both of CG and contact point is strong. For the yaw-axis of the struck object the strongest effect is observed for stronger misalignments of CG and contact point as long as both CGs and the contact point are colinear. For the striking object either but not both misalignments lead to a strong effect of different sign.
Considering the off-diagonal percentage a strong linear correlation (or anti-correlation) across all geometric arrangements is observed for all axes except yaw of the striking object (correlation coefficients: $x_{\text{struck}} = 0.93$, $y_{\text{struck}} = -0.85$, $yaw_{\text{struck}} = 0.82$, $x_{\text{striking}} = -0.93$, $y_{\text{striking}} = 0.85$, $yaw_{\text{striking}} = 0.32$). Figure 7 explains the latter by the observed sign change for different geometries.

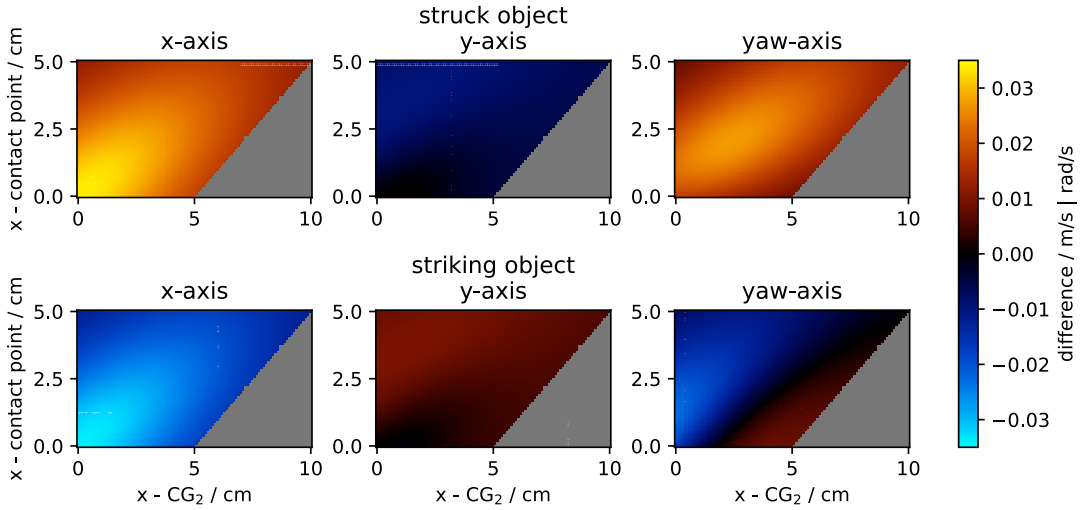

Fig 7: Difference between baseline and new method for 10% off-diagonal values of the added mass tensor as a function of geometric arrangement. y-axis scaled by 20 for visibility.

Experimental Validation

From the collision experiments, the measured change of velocity in all 6 DOF was determined. Moreover, all quantities to predict the velocity change with the theory developed in this paper were

determined: pre-collision velocity vector, CG of floating dock and PSV, point of contact, contact normal, and CoR. The added mass tensors for dock and PSV were determined by computer simulation using WAMIT (see appendix A). Given the small values of the off-diagonal terms of the added mass tensor for both floating dock and PSV, using our new model only produces slightly different results compared to a model using solely the diagonal added mass tensor. As such the focus of the following analysis is the ability of our model to predict experimental collision responses correctly.

The data (Fig. 8) was compared to the theory by use of correlation coefficients (in parenthesis), which reveal a good agreement between measurement and theory for the following linear modes: x-axis (dock: 0.85, PSV: 0.86), y-axis (dock: 0.63, PSV: 0.70) and yaw-axis (dock: 0.61, PSV: 0.15), with the yaw-axis for the PSV being an outlier of that trend. The agreement between measurement and theory for the following oscillatory modes (see appendix B) overall is low: z-axis (dock: -0.05, PSV: -0.31), $roll$-axis (dock: -0.38, PSV: -0.27) and $pitch$-axis (dock: -0.17, PSV: 0.16). A more detailed look reveals that the theory generally underestimates the velocity changes along all axis, except for the roll-axis of the PSV. This effect is smaller for the linear modes, where the correct trend for the velocity changes was identified and stronger for the oscillatory modes.

The same trends as described before are observed if only a subset of the experiments based on the experimental conditions is analyzed. The only notable difference is the subset of lower thrust power for the floating dock, for which larger positive correlations are observed for the oscillatory modes as well (z: 0.34, $roll$: 0.21, $pitch$: 0.37).

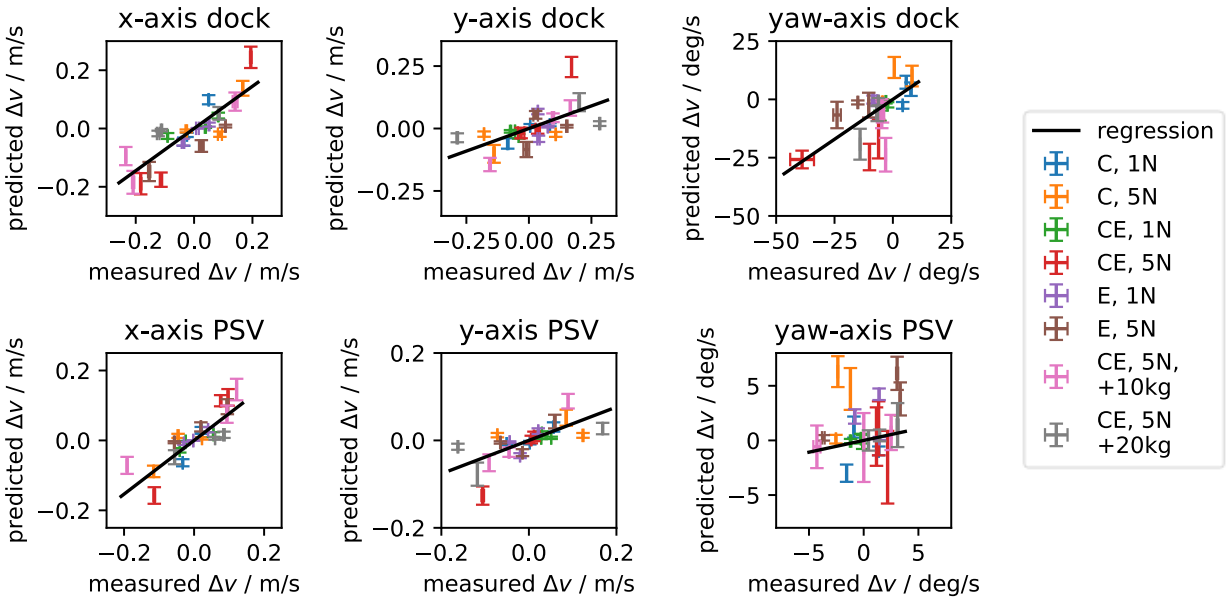

Figure 8: Measured and predicted velocity changes for the linear modes at different experimental parameters together with the respective regression lines.

DISCUSSION

To the best of our knowledge, this work is the first to present a collision resolution algorithm that takes the full added mass tensor into account. This novel theory was obtained by applying a common formalism for the equations of motion in the marine domain to a well-established algorithm for collision resolution in the field of computational physics.
The conducted parameter study shows that even at small to moderate values of the off-diagonal elements of the added mass tensor, the velocity change upon a collision changes significantly compared

to solely using the diagonal elements of the tensor. The parameter study further indicates that in certain geometric situations motions along an axis can be captured that the currently prevalent theory in the literature simply can not capture. Generally, the geometric arrangement has a strong influence on how the velocity changes along certain axes. This effect shows a complex interplay with the coupling terms between the axes, when they are considered.

Our new theory shows good performance in predicting real collision events between a floating dock and the PSV ship model for the linear modes of motion. The predictive performance is severely reduced for the oscillatory modes of motion. The latter is attributed to two main effects. Firstly, both floating dock and PSV model are rather stable floating objects, making the collision response along the oscillatory modes both small and short-lived and thus difficult to both accurately measure and correctly predict. Secondly, the model presented in this paper solely deals with the inertial collision response at a single point of contact over an infinitesimal time. As such, additional effects like waves, friction, prolonged contact and extended contact areas are not captured by the presented theory. That such effects are indeed present is further supported by the persistent underestimation of the measured collision response by our theory, which indicated the presence of additional effects. Moreover, the prediction of the oscillatory modes for the floating dock was better at lower thrust forces of the PSV, which points to wave effects causing some of the disagreement between measurement and theory, since more energy put into the water by higher thrusts leads to stronger disturbances of the free surface.

CONCLUSIONS

In this work, a new theory and algorithm to resolve collision events between floating objects that uses the full added mass tensor was introduced. A parameter study was conducted to investigate the difference between the new theory and the currently most used method in the literature. The theory was further used to predict velocity changes for experimentally observed collisions and the results were compared with the actual measurements.

To predict the velocity change upon a collision, the pre-collision velocity vectors, CoR, geometric arrangement (CG, contact point, contact normal), and system inertia tensors of the colliding objects must be known. For the parameter study restrictions were made to the geometry, and the system inertia tensors was predicted using the WAMIT software (a panel method). A significant difference between the reference method and our theory was observed in the parameter study. In future work, the restrictions to the geometry of the collisions could be lifted to gather an even more complete picture of the interplay between the inputs to the collision resolution algorithm. Moreover, more realistic objects could be studied in addition to the cubes augmented with artificial added mass used here.

The comparison between experimental data and theoretical predictions showed good agreement for the linear modes of motion and weak agreement for the oscillatory modes. This shows our method is generally capable of predicting the velocity changes due to real collision events of floating objects. To compensate for the additional effects causing the observed deviations, our method should be augmented with the capability to handle frictional effects during the collision as well. Further it should be evaluated in a simulation that captures wave effects to see if the prediction in the oscillatory modes is significantly improved.

Finally, future work could develop the theory presented here to naturally support a 3 DOF geometry, since the full theory currently needs to be used since singular matrices are otherwise encountered during inversions. Since the predictive capabilities of the method for real world collisions are particularly good for the linear modes of motion, this endeavour seems worthwhile.

ACKNOWLEDGEMENTS

The authors thank Robert Gash for his support in collecting the experimental data for this work and the NRC and particularly their staff Jason Murphy, Grant Hickey and Derek Butler for facilitating the experiments in their offshore engineering basin research facility. We further are grateful to the Ocean Frontier Institute for their financial support of Marius Seidl in the framework of the Ocean Graduate Excellence Network.

REFERENCES

Baraff, D, & Witkin, A., 1997. Physically Based Modeling: Principles and Practice. *SIGGRAPH 1997 Course Notes*, pp.D32-D68.

Fossen, T. I., 2002. Marine Control Systems – Guidance, Navigation, and Control of Ships, Rigs and Underwater Vehicles. Marine Cybernetics: Trondheim.

Korotkin, A. I., 2009. Added Masses of Ship Structures. Springer-Verlag:Berlin.

Liu, B., & Soares, C. G., 2023. Recent developments in ship collision analysis and challenges to an accidental limit state design method. *Ocean Engineering*. 270, p.113636

Liu, Z., & Ahmdahl, J., 2010. A new formulation of the impact mechanics of ship collisions and its application to a ship–iceberg collision. *Marine Structures*. 23(3), pp.360-384.

Liu, Z. & Ahmdahl, J. 2019. On multi-planar impact mechanics in ship collisions. *Marine Structures*. 63, pp.364-383.

Seifried, R., Schiehlen, W., & Eberhard, P., 2010. The role of the coefficient of restitution on impact problems in multi-body dynamics. *Proceedings of the Institution of Mechanical Engineers, Part K: Journal of Multi-body Dynamics*, 224(3), pp.279-306.

Song, M., Kim, E., Amdahl, J., Ma, J., & Huang, Y., 2016. A comparative analysis of the fluid-structure interaction method and the constant added mass method for ice-structure collisions. 49, pp.58-75.

Petersen, M. J., 1982. Dynamics of ship collisions. *Ocean Engineering*. 9(4), pp.295-329.

Pfeiffer, F., & Glockner, C., 1996. *Multibody Dynamics with Unilateral Contacts.* WILEY-VCH Verlag: Weinheim.

Yu, Z., Ahmdahl, J., & Storheim, M., 2016. A new approach for coupling external dynamics and internal mechanics in ship collisions. *Marine Structures*. 45, pp.110-132.

Yu, Z. Shen, Y., Amdahl, J., & Greco, M., 2016b. Implementation of Linear Potential-Flow Theory in the 6DOF Coupled Simulation of Ship Collision and Grounding Accidents. *Journal of Ship Research*. 60(3), p.119

WAMIT, Inc., 2025. WAMIT USER MANUAL Version 7.5. http://www.wamit.com/manual7.x/v75_manual.pdf (online, accessed Jan 10, 2025).

APPENDIX A

Values of the added mass tensor of the floating dock

$$\mathbf{M}_{\mathrm{A,dock}} = \begin{bmatrix} 1.81\ \mathrm{kg} & 0\ \mathrm{kg} & 0\ \mathrm{kg} & 0\ \mathrm{kg \cdot m} & 1.58\ \mathrm{kg \cdot m} & 0\ \mathrm{kg \cdot m} \\ 0\ \mathrm{kg} & 1.81\ \mathrm{kg} & 0\ \mathrm{kg} & -1.58\ \mathrm{kg \cdot m} & 0\ \mathrm{kg \cdot m} & 0\ \mathrm{kg \cdot m} \\ 0\ \mathrm{kg} & 0\ \mathrm{kg} & 269\ \mathrm{kg} & 0\ \mathrm{kg \cdot m} & 0\ \mathrm{kg \cdot m} & 0\ \mathrm{kg \cdot m} \\ 0\ \mathrm{kg \cdot m} & -1.32\ \mathrm{kg \cdot m} & 0\ \mathrm{kg \cdot m} & 9.36\ \mathrm{kg \cdot m^2} & 0\ \mathrm{kg \cdot m^2} & 0\ \mathrm{kg \cdot m^2} \\ 1.25\ \mathrm{kg \cdot m} & 0\ \mathrm{kg \cdot m} & 0\ \mathrm{kg \cdot m} & 0\ \mathrm{kg \cdot m^2} & 9.63\ \mathrm{kg \cdot m^2} & 0\ \mathrm{kg \cdot m^2} \\ 0\ \mathrm{kg \cdot m} & 0\ \mathrm{kg \cdot m} & 0\ \mathrm{kg \cdot m} & 0\ \mathrm{kg \cdot m^2} & 0\ \mathrm{kg \cdot m^2} & 0.195\ \mathrm{kg \cdot m^2} \end{bmatrix} \tag{15}$$

and the PSV model

$$\mathbf{M}_{\mathrm{A,PSV}} = \begin{bmatrix} 2.78\ \mathrm{kg} & 0\ \mathrm{kg} & 4.32\ \mathrm{kg} & 0\ \mathrm{kg \cdot m} & 4.79\ \mathrm{kg \cdot m} & 0\ \mathrm{kg \cdot m} \\ 0\ \mathrm{kg} & 21.0\ \mathrm{kg} & 0\ \mathrm{kg} & -0.54\ \mathrm{kg \cdot m} & 0\ \mathrm{kg \cdot m} & 0.51\ \mathrm{kg \cdot m} \\ 4.21\ \mathrm{kg} & 0\ \mathrm{kg} & 122\ \mathrm{kg} & 0\ \mathrm{kg \cdot m} & 8.89\ \mathrm{kg \cdot m} & 0\ \mathrm{kg \cdot m} \\ 0\ \mathrm{kg \cdot m} & -0.57\ \mathrm{kg \cdot m} & 0\ \mathrm{kg \cdot m} & 0.49\ \mathrm{kg \cdot m^2} & 0\ \mathrm{kg \cdot m^2} & -0.063\ \mathrm{kg \cdot m^2} \\ 4.99\ \mathrm{kg \cdot m} & 0\ \mathrm{kg \cdot m} & 11.3\ \mathrm{kg \cdot m} & 0\ \mathrm{kg \cdot m^2} & 16.1\ \mathrm{kg \cdot m^2} & 0\ \mathrm{kg \cdot m^2} \\ 0\ \mathrm{kg \cdot m} & 0.87\ \mathrm{kg \cdot m} & 0\ \mathrm{kg \cdot m} & 0.12\ \mathrm{kg \cdot m^2} & 0\ \mathrm{kg \cdot m^2} & 4.63\ \mathrm{kg \cdot m^2} \end{bmatrix} \tag{16}$$

as predicted by WAMIT.

APPENDIX B

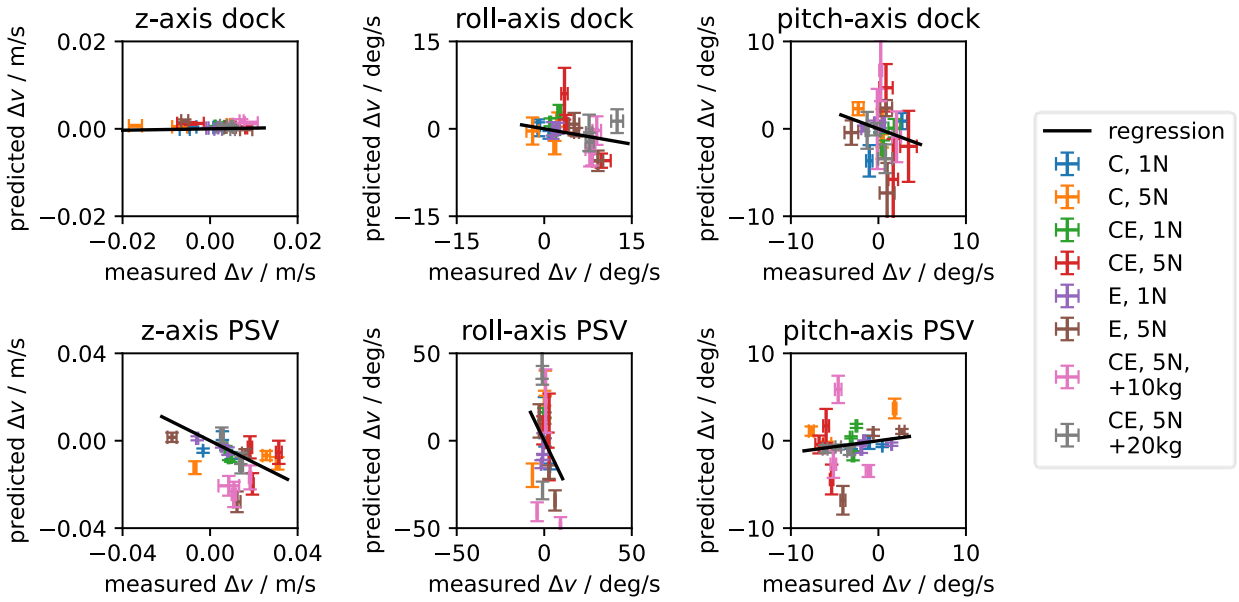

Figure 9: Measured and predicted velocity changes for the oscillatory modes at different experimental parameters together with the respective regression lines.